Technology in Cancer Research and Treatment
ISSN 1533-0346
Volume 10, Number 1, February 2011

Calibration of Elekta aSi EPIDs Used as Transit Dosimeter

www.tcrt.org

S. Cilla, Ph.D.[1]
A. Fidanzio, Ph.D.[2]
F. Greco, Ph.D.[2]
D. Sabatino, Ph.D.[1]
A. Russo, Ph.D.[3]
L. Gargiulo, Ph.D.[2]
L. Azario, Ph.D.[2]
A. Piermattei, Ph.D.[1,2]*

[1]U.O di Fisica Sanitaria, Centro di Ricerca e Formazione ad Alta Tecnologia nelle Scienze Biomediche, Università Cattolica del Sacro Cuore, Campobasso, Italy
[2]Istituto di Fisica, Università Cattolica del Sacro Cuore, Largo F. Vito 1, 00168, Rome, Italy
[3]U.O. di Radioterapia, Casa di cura Marco Polo USI, Rome, Italy

The transit *in vivo* dosimetry performed by the Electronic Portal Imaging Device (EPID), avoids the problem of solid-state detector positioning on the patient. Moreover, the dosimetric characterization of the recent Elekta aSi EPIDs in terms of signal stability and linearity enables these detectors adaptable for the transit *in vivo* dosimetry with 6, 10 and 15 MV photon beams. However, the implementation of the EPID transit dosimetry requires several measurements. Recently, the present authors have developed an *in vivo* dosimetry method for the 3D CRT based on correlation functions defined by the ratios between the transit signal, s_t (w,L), by the EPID and the phantom mid-plane dose, D_m(w,L), at the Source to Axis Distance (SAD) as a function of the phantom thickness, w, and the square field dimensions, L. When the phantom mid-plane was positioned at distance d from the SAD, the ratios s_t(w,L)/s'_t(d,w,L), were used to take into account the variation of the scattered photon contributions on the EPID as a function of, d and L. The aim of this paper was the implementation of a procedure that uses generalized correlation functions obtained by nine Elekta Precise linac beams. The procedure can be used by other Elekta Precise linacs equipped with the same aSi EPIDs assuring the stabilities of the beam output factors and the EPID signals. The calibration procedure of the aSi EPID here reported avoids measurements in solid water equivalent phantoms needed to implement the *in vivo* dosimetry method in the radiotherapy center. A tolerance level ranging between ±5% and ±6% (depending on the type of tumor) was estimated for the comparison between the reconstructed isocenter dose, D_{iso} and the computed dose $D_{iso,TPS}$ by the treatment planning system (TPS).

Key words: *In vivo* dosimetry; Electronic portal imaging device; Dosimetry; Radiotherapy.

Introduction

The dose reconstructions performed during the treatment are compared to an expected dose supplied by the treatment planning system (TPS) to check the presence of discrepancies due to errors by data transfer from the TPS to the radiotherapy unit in the functioning of the treatment equipment, and the accuracy of the dose calculation algorithms employed by the TPS and errors due to the patient set-up or patient morphology changes.

A standard *in vivo* dosimetry technique is based on the entrance dose reconstruction using a solid state detector on the patient surface (1). These *in vivo* dosimetry techniques are generally applied only for an initial check because they require workload for detector positioning and corrections for their x-ray fluence absorption.

The increasing complexity of techniques in radiotherapy requires an accurate verification of the dose delivered to the patient and several researches have been

Corresponding Author:
Angelo Piermattei, Ph.D.
E-mail: a.piermattei@rm.unicatt.it

addressed to pre-treatment dose verification for intensity modulation radiotherapy (IMRT) and to reconstruct the delivered patient dose during the treatment by means of electronic portal imaging devices (EPIDs) (2, 3, 4). As respect to the traditional EPIDs such as fluoroscopic screen/camera-based and liquid-filled matrix ionization chambers, the new generation of EPIDs, equipped with amorphous silicon (aSi) flat panels, supply more stable transit signals and are suitable as transit detectors. Recently, the authors have developed an *in vivo* dosimetry method based on correlation functions defined by the ratios between the transit signal, s_t, measured by aSi EPIDs, and the solid water phantom mid-plane doses, D_m, measured by an ion-chamber positioned along the central axis (5).

The aim of the present paper has been the determination of the generalized correlation functions for the recent Elekta IviewGT aSi EPIDs needed to implement an *in vivo* transit dosimetry method for the 3D conformed radiotherapy (3DCRT). This way, the efforts for the measurements in solid water-phantom, needed to implement the method in other centres are avoided.

Materials and Methods

Linac Units

In this work, 9 x-ray beams of 6, 10 and 15 MV supplied by three Elekta Precise linacs (Elekta, Stockholm, Sweden) have been used to obtain the generalized correlation functions for the implementation of an *in vivo* dosimetry method. Table I reports some characteristics of the linacs examined in this work operating at the Università Cattolica del Sacro Cuore (UCSC) of Campobasso and at the Unione Sanitaria Internazionale (USI) of Rome. The linacs were equipped with EPIDs IviewGT Elekta, based on the aSi panel XRD 1640 AL5 (PerkinElmer Optoelectronics, Fremont, CA USA). The sensitive layer is based on aSi sensors operating as a two-dimensional photodiode array. The sensitive layer consists of 1024 × 1024 pixels with a pitch of 400 μm, resulting in an active area of 409.6 × 409.6 mm^2. Back-projected at the source-axis distance (SAD), this corresponds to an area of 259 × 259 mm^2 and a pitch of 253 μm. A more detailed description of the functionality and basic properties of such devices is reported in literature (6, 7). Above the detector, a copper plate with a thickness of 1 mm, acts as build-up material and the copper plate source-EPID distance (SED) is fixed around 159 cm (table I). However, the EPID can be in a retracted position when its use is not required. The Elekta Precise linacs were equipped with a multileaf collimator (MLC) that consists of two opposed banks carrying 40 leafs each with a 1 cm width at the isocenter. The x-ray beams were calibrated following the IAEA 398 protocol (8) using a 10 × 10 cm^2 field size at the source-phantom distance (SSD) equal to 100 cm, coincident with the SAD. At the reference depth z_{ref} equal to 10 cm in water phantom, the reference dose was equal to 1cGy/MU for the UCSC beams while the beams at the USI were calibrated with 1cGy/MU at the depth of maximum dose, d_{max}.

Table I
Source EPID distances, SED, and the index quality $TPR_{20,10}$ for the three linac used in this work.

	SED (cm)	6 MV	10 MV	15 MV
Linac A (UCSC)	159.0	0.683	0.730	0.759
Linac B (UCSC)	159.5	0.683	0.731	0.759
Linac C (USI)	158.2	0.686	0.736	0.760

The quality index of each beam was obtained by the tissue phantom ratios $TPR_{20,10}$, (6) here named TPR, measured as the ratio between the doses at the water depth of 20 cm and 10 cm, respectively, with an accuracy of 0.3% (Table I).

Implementation of the Transit Dosimetry

The *in vivo* dose reconstruction method here reported, is based on a set of measurements of (i) dose values by a cylindrical ion-chamber PTW, model TM31010 (PTW Freiburg, Germany) positioned at the SAD along the beam central axis coincident with the mid-plane of a solid water-equivalent phantom, (SWEP) (Gammex MIDDLETON, WISCONSIN 53562-0327, USA.), and (ii) the transit signal by the EPID below the SWEP at the SED, measured on the beam central axis. The measurements have been carried out using phantom thicknesses w = 10, 22, 30 and 42 cm, and square field sides L = 4,8,10,12,16 and 20 cm defined at the SAD. Each measurement was obtained with 100 MU supplied with the clinical monitor unit rate 400 MU/min, which was used at the UCSC, and 200 MU/min used at the USI.

Figure 1A shows the experimental set-up used to determine, for every TPR, the mid-plane doses per MU, D(TPR,w,L), and the transit signals per MU, s_t(TPR, w, L). Figure 1B shows an experimental set-up used to measure the transit signals per MU, s_t(TPR,w,L,d), when the phantom mid-plane was shifted a distance, d, from the SAD. These last values were used to determine the empirical factors f(TPR,d,L)

$$f(TPR,d,L) = s_t\,(TPR,w,L)/s_t\,(TPR,w,L,d) \qquad [1]$$

that takes into account the variations of the scattered photon contributions on the EPID due to the different mid-plane phantom positions as respect to the SAD. In previous papers (9, 10) it was shown that, for distances, d, in the range of ±7 cm, the f(TPR,d,L) factors were independent of the thickness

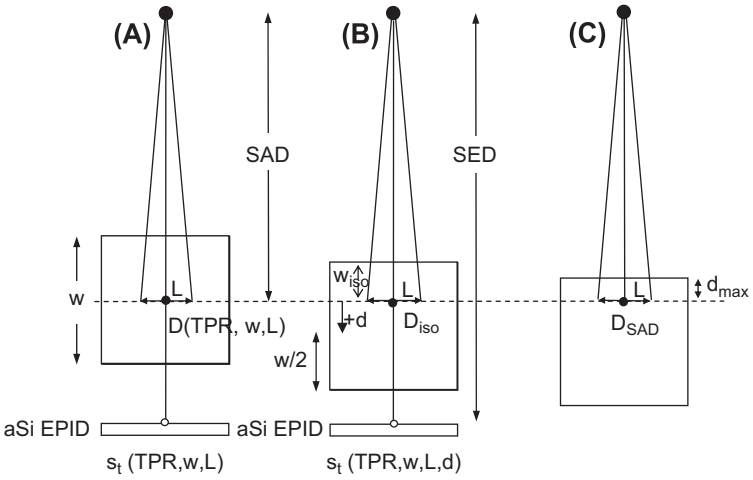

Figure 1: Set-up used to measure the phantom mid-plane doses, D(TPR,w/2,L), and the EPID transit signals s_t(TPR,w,L) and s_t(TPR,w,L,d). w is the phantom thickness, L is the side of the square field and the SED is the source to EPID distance. (**A**) Reference configuration with the phantom mid-plane at the source to axis distance SAD = 100 cm. The ion chamber was positioned at the phantom mid-plane (●) to determine D(TPR,w,L), while s_t(TPR,w,L) was measured in the point (○) on the beam central axis; (**B**) the phantom mid-plane is at the distance, d, below the SAD. The dose, D_{iso}, at the isocenter point can be obtained by equation [3]; (**C**) phantom set-up used to determine the D_{SAD} at the depth, d_{max}, of the maximum dose for a 10 × 10 cm^2 field.

w within ±0.5%. This allowed to report the factors in equation (1) as a function of, d, and L, for every quality beam.

Defining the correlation function F(TPR,w,L) as the ratios

$$F(w,L) = \frac{s_t(TPR,w,L)}{D(TPR,w,L)} \quad [2]$$

the dose D(TPR,w_{iso},L) at depth w_{iso} can be determined (referring to figure 1) by

$$D(TPR,w_{iso},L) = S_t(TPR,w,L,d) \times \left[\frac{f(TPR,d,L)}{F(TPR,w,L)} TMR_{w/2}^{w_{iso}}(L)\right] \quad [3]$$

where S_t(TPR,w,L,d) is the integral transit signal and the $TMR_{w/2}^{w_{iso}}(L)$ is the ratio between the Tissue Maximum Ratios evaluated at the depths, w_{iso}, and w/2, respectively. The accuracy of equation [3] was estimated equal to ± 4.5% also in inhomogeneous phantoms where, w, was obtained in terms of radiological thickness (7, 8).

The correlation functions F(TPR,w,L) of the equation [2] had to be determined for every linac beam because they depend on the beam MU calibration and on the EPID sensitivity of the centers.

The aim of this work has been the determination of the generalized data for the ratios in equation [2] dependent, for every couple of (w,L), on the beam quality index TPR.

Dose Measurements at Mid-Plane

A water equivalency correction factor k_{WE} for the SWEP was determined as the ratio between the chamber reading in natural water and that in solid phantom, at the same linear depth of 10 cm for the 6 MV, 10 MV and 15 MV photon beams with a field 10 × 10 cm^2 in size. So the ion-chamber reading in SWEP, was multiplied for the factor, k_{WE}, before applying the IAEA code (6) to obtain the dose to water.

The beam MU calibration may be different between various Centers. To take into account this problem a factor, k_o, was defined as the ratio between two dose values at the depth, d_{max}, coincident with the SAD (figure 1c) for a field 10 × 10 cm^2

$$k_0 = D^0_{SAD}/D_{SAD} \quad [4]$$

where D^0_{SAD} = 1 cGy/MU and D_{SAD} is the specific dose of the beam, measured in the center. Multiplying D(TPR,w,L) by k_o

$$D^0(TPR,w,L) = D(TPR,w,L)\cdot k_0 \quad [5]$$

a set of dose per MU values, D^0(TPR,w,L), in terms of cGy/MU, independent of the MU calibration adopted by the two centers, were obtained. In other words for every couple of data (w,L) the dose per MU obtained by equation [5] resulted dependent on the TPR index only.

Portal Imaging Measurements

An Elekta aSi EPID frame is defined as the raw signal s'(x,y) from one readout of the entire EPID panel, where x and y indicate the matrix pixel coordinates. Every frame is generated in 434 ms. The portal images are obtained by the integrated signals over the total beam time, multiplied by a pixel scaling factor, (PSF), to produce a quality image (11). The pixel signals are stored as a 16-bit number and result inversely proportional to the dose. In this work, the portal images have been evaluated using an in-house developed software in Matlab version 7.1 (The Mathworks Inc., Nantick, Massachussets) environment. The IviewGT

software (version 3.3) supplied the PSF value, that in this work was used to obtain the integrated pixel values s(x,y) by subtracting the pixel values s'(x,y) from the number 65535 (2^{16}-1) and then dividing it by the PSF, according to equation

$$s(x,y) = \frac{65535 - s'(x,y)}{PSF} \quad [6]$$

In particular, in this paper the EPID signal, s (at the SED), on the beam central axis, in terms of arbitrary units (au), was obtained by the average of the s(x,y) supplied by the 12 × 12 central pixels (an area of 4.8 × 4.8 mm^2) around the beam central axis.

The signals, s, were obtained for 6 MV, 10 MV and 15 MV beams supplied by the 3 linacs, using a 10 × 10 cm^2 field at the SAD and delivering 100 MU each time. This way the reproducibility of the EPID signals was checked taking into account the daily linac output fluctuations. Moreover, the EPID dependence on the dose rate was investigated changing the dose rate supplied by the linac (50, 100, 200 and 400 MU/min), while to assess the signal s linearity with MUs, the signal s_{MU}, obtained delivering 5, 20, 50, 100, 200 and 400 MUs, was used to determine the linearity correction factor, k_{lin}, defined as

$$k_{lin} = \frac{s}{s_{MU}} \quad [7]$$

where, s, is the signal per MU obtained for 100 MUs.

Moreover, the ghosting effect that represents an artifact in the image, due to signals present in frames subsequent to the frame in which it has been generated, has been measured following the Van Esch approach (4).

The aSi EPIDs operating in the centers can supply different values of s for the same delivered dose and this yield can change in time. Moreover, by a private communication of the Elekta the fixed SEDs for different Precise linacs equipped with the aSi EPIDs ranged between 158.2 cm and 159.8 cm.

In this paper a procedure that assures a stable calibration of the aSi EPIDs has been proposed. The first step was the determination of the $\bar{s}$, in terms of au/MU, as the mean value of the s per MU obtained in the long term (six months) reproducibility checks for a 10 × 10 cm^2 field at the SAD and delivering 100 MUs. In a second step the $\bar{s}$ signal was converted in a centi-CU per MU (cCU/MU), assuming that the $\bar{s}$ in au/MU was equal to 1 cCU/MU. This means that, at the SED, a sensitivity factor, k_s, in terms of cCU/au, was defined as

$$k_s = \frac{1}{\bar{s}} \quad [8]$$

This way an integral signal, s in terms of au, (obtained by a number of MU), if multiplied by, k_s, can be read in terms of cCU and this reading is independent on (i) the EPID sensitivity and (ii) the MU calibration of the megavoltage beam. In conclusion, aSi EPIDs with different sensitivities operating in different centers at a fixed SED (approximately 159 cm), can supply, for every MU, the same $s \cdot k_s$ reading. Of course, if the signal, s, changes over a tolerance level from the $\bar{s}$, a new, k_s factor should be adopted to take into account the change of the EPID sensitivity.

The measured transit signals per MU, $s_t(TPR,w,L)$, (obtained with the SWEP on the beam) were multiplied by, k_s

$$S^0_t(TPR,w,L) = s_t(TPR,w,L) \cdot k_s \quad [9]$$

obtaining generalized $s^0_t(TPR,w,L)$ values, independent of both the MU calibration and the EPID sensitivity, but dependent on the TPR index only.

Moreover, the measurements of the $s_t(TPR,w,L,d)$ values were carried out positioning the phantom mid-plane below and above the SAD, at distances, d, up to ±7 cm, as a function of, w, and, L. These last data were used to determine the f(TPR,d,L) factor defined by equation (1).

D_{iso} Reconstruction

A commercial software package (TableCurve 3D; SPSS-Science, 2000) was used to find the surfaces of best fit to the measured data values for the generalized doses $D^0(TPR,w,L)$ and the generalized transit signals $s^0_t(TPR,w,L)$. The tableCurve 3D is a linear and non-linear surface-fitting software package that automates the surface-fitting process and, in a single processing step, instantly fits and ranks about a thousand equations enabling users to find the ideal model to their 3D data within seconds. In this software, both linear and non-linear equations can minimize the sum of squares of the residuals, where a residual is simply the difference between the z value of a given x,y,z triplet and the z value computed from the surface-fit equation at this same x and y value. In other words, a residual is the vertical z-distance between the surface and a data point, and it can be either positive or negative in value. The square of a residual is always positive, and thus reflects the magnitude of the residual (12).

The generalized mid-plane doses $D^0(TPR,w,L)$ (equation 5) were fitted by the surface equations as

$$D^0(TPR,w,L) = a_1 + a_2\,TPR + a_3\,w + a_4\,TPR^2 + a_5\,w^2 + a_6\,TPR\,w \quad [10]$$

where the six adjustable coefficients ai (i = 1,..,6) are real numbers obtained through the fitting procedure.

The generalized transit signals $s^0_t(TPR,w,L)$ (equation 9) were fitted by the surface equations:

$$s^0_t = b_1 + b_2TPR + b_3w + b_4TPR^2 + b_5w^2 + b_6TPRw + b_7TPR^3 + b_8w^3 + b_9TPRw^2 + b_{10}TPR^2\,w \quad [11]$$

where the ten adjustable coefficients bi (i = 1,..,10) are real numbers obtained through the fitting procedure.

We have choose polynomial equations as a matter of simplicity. The number of adjustable parameters (6 or 10) were chosen as the minimum numbers that can provide residual values (*i.e.* the differences between the surface and experimental data) well within ±1.0% for D^0 and within ±1.5% for s^0_t.

In clinical practice, the dose $D(TPR,w_{iso},L)$ in cGy for a beam quality index TPR named D_{iso} for simplicity can be rewritten by equation [3] as

$$D_{iso} = S_t(TPR,w,L,d) \times \frac{k_s k_{lin}}{k_0} \times \left[\frac{f_{MV}(d,L)}{F^0(TPR,w,L)} \times TMR^{w_{iso}}_{w/2} \right] \quad [12]$$

where $S_t(TPR,w,L,d)$, is the transit integral signal in terms of au, obtained by the EPID for the MU, used for a specific beam. This signal is converted by the sensitivity factor, k_s, in cCU, and corrected by the factors k_{lin} and k_0; $F^0(TPR,w,L)$ is the ratio $s^0_t(TPR,w,L)/D^0(TPR,w,L)$ obtained by the equations [10] and [11]; $f_{MV}(d,L)$ are the factors obtained by equation [1] averaging the data for the same MV.

The parameters, w, w/2, w_{iso}, and d, present in equation [12] can be obtained following two steps, i) the patient's CT scan containing the isocenter was used to measure, along the beam central axis, the patient's geometrical thickness, t, the distance, d, and the isocenter depth, d_{iso}; ii) calibrated CT numbers were used to determine the mean relative electronic density along the patient's thickness, t, and, d_{iso}, (that are generally supplied automatically by the TPS). Therefore, the water-equivalent or radiological thickness, w, and the depth, w_{iso}, can be determined as the product of, t, and, d_{iso}, by the relative mean physical densities, obtained by the linear relation between the electronic density and the physical density (13). The equivalent square field is generally supplied automatically by some TPSs, otherwise it can be obtained by the Sterling approximation (14).

Results

Factors $f_{MV}(w,L)$

The f(TPR d,L) factors (by equation 1) resulted about independent (within 0,2%) of the TPR of the beams with the same MV. Figure 2 shows the $f_{MV}(d,L)$ average factors obtained for the 15 MV photon beams as a function of the distance, d, for some square fields (L = 4,10,16,20 cm). These factors were fitted with linear equations as a function of the distance, d

$$f_{MV}(d,L) = f_1 d + 1 \quad [13]$$

The coefficients f_1 of the linear fits are reported in Appendix A.

In clinical cases, once determined the distance, d, between the isocenter point, the middle patient thickness and the equivalent square field, L, of the beam characterized by the MV value, the $f_{MV}(d,L)$ factor can be determined by interpolation of the data reported in figure 2.

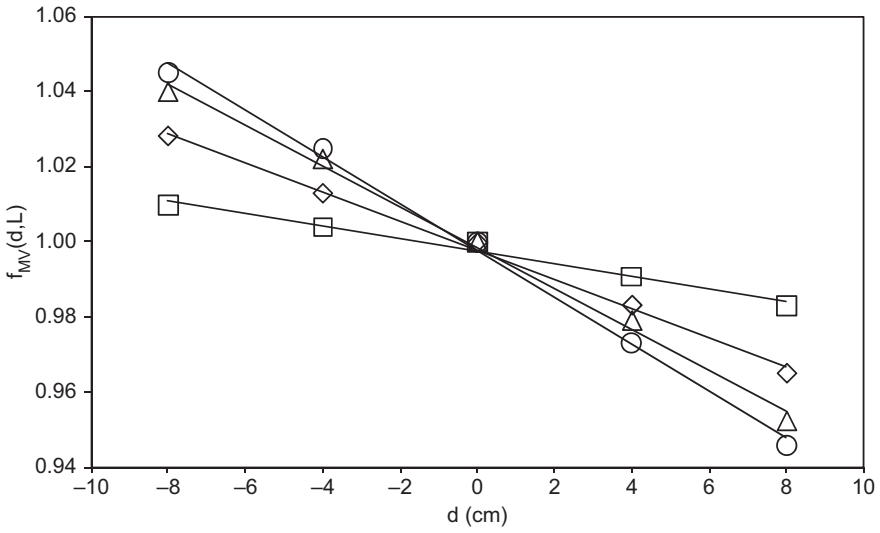

Figure 2: $f_{MV}(d,L)$ factors obtained for 4 × 4(□), 10 × 10(◇), 16 × 16 (Δ) and 20 × 20 cm^2 (○) square fields of 15 MV, and the linear fit (continuous lines) by equation [13].

Table II
k_0 factors (equation 4) obtained for the 9 beams of the three linacs examined in this work.

	Linac A	Linac B	Linac C
6 MV	0.660	0.660	0.971
10 MV	0.701	0.701	0.952
15 MV	0.723	0.723	0.943

Determination of Generalized Correlation Ratios

Generalized Mid-Plane Doses

Table II reports the k_0 factors determined for the nine photon beams of the three linacs examined in this work.

Figure 3 shows the D^0(TPR,w,L) values for different w thicknesses as a function of the TPRs for the 16×16 cm^2 square field. The data are reported with the TPR uncertainty (bars of 0.3%). The dose uncertainty was estimated about 2.5% and it is represented by the symbol's sizes. A good linearity is shown with correlation indexes $R \geq 0.998$. The same results were found for the other field dimensions.

Figure 4 shows the surfaces fitting the dose D^0 (TPR,w,L) by equation [10] for some square field dimensions used in this paper.

In Appendix A are reported the 6 coefficients a_i (i = 1,..,6) for the best-fit of the surface equations.

The differences between the experimental data and the computed data by equations (10) were within 1.0% (2 SD) with maximum residuals up to 1.4%.

Generalized Transit Signals

The $\bar{s}$ values obtained by the three aSi EPIDs in long-term periods for the three quality beams showed a dispersion index of 2 % (2 SD), confirming the results obtained in other works, (15) while in the short term (during the measurement session) the dispersion was 1% (2 SD). Table III reports the k_s factors obtained for the 9 beams of the three linacs used in this work.

Table IV reports for the three linacs the average values of the correction factors, k_{lin}, for the beams with a 0.5% (2 SD). These factors resulted independent from the MU/min used.

The amount of ghosting effect for the three aSi EPIDs was evident only for very high number of MUs delivered far from those used in clinical fields, so a ghosting contribution less than 1% was estimated for a number of MUs no greater than 200, and in this work this effect was neglected.

Figure 5 shows the s^0_t(TPR,w,L) values for different w thickness as a function of the TPRs for the 16 × 16 cm^2 square field. The data are reported with the TPR uncertainty (bars of 0.3%). The dose uncertainty was estimated about 3% and it is represented by the symbol's size. A good linearity is shown, with correlation indexes $R \geq 0.997$. The same results were obtained for the other beams.

Figure 6 shows the surfaces fitting the s^0_t(TPR,w,L) by equation [11] for some square fields used in this paper. In Appendix A are reported the coefficients b_i (i = 1,….10) for the best-fit of the surface equations. The differences between the experimental data and the computed data by equations (11) were within 1.5% (2 SD) with maximum residuals up to 2.0%.

Correlation Ratios F^0(TPR,w,L) for a Clinical Case

For each beam of quality index TPR used for patient treatment, a radiological patient's thickness, w, was determined and six generalized mid-plane doses and the six generalized transit signals, once for every square field size (section 2.2), were obtained by equations [10] and [11] These data were fitted to obtain by interpolation the data s^0_t(TPR,w,L) and D^0(TPR,w,L) for the patient-equivalent square field.

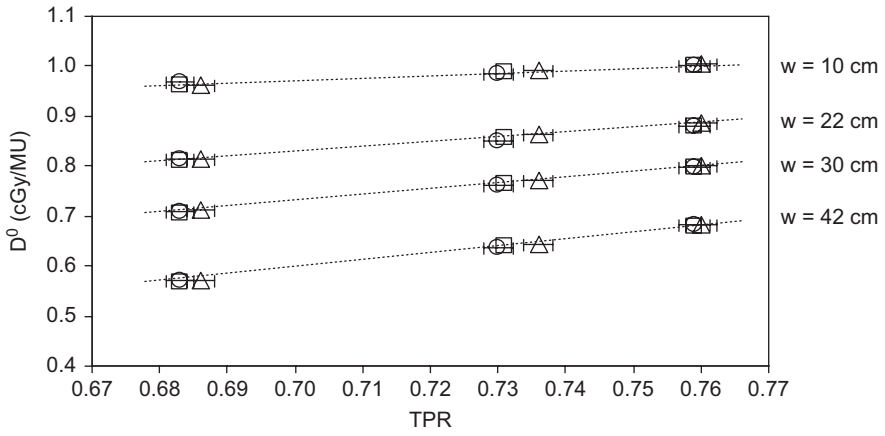

Figure 3: D^0(TPR,w,L) values and the linear fits obtained for w = 10,22,30 and 42 cm as a function of TPR for the 16 × 16 cm^2 square field. The symbols refer to linac A (□), linac B (○) and linac C (Δ) in Table 1.

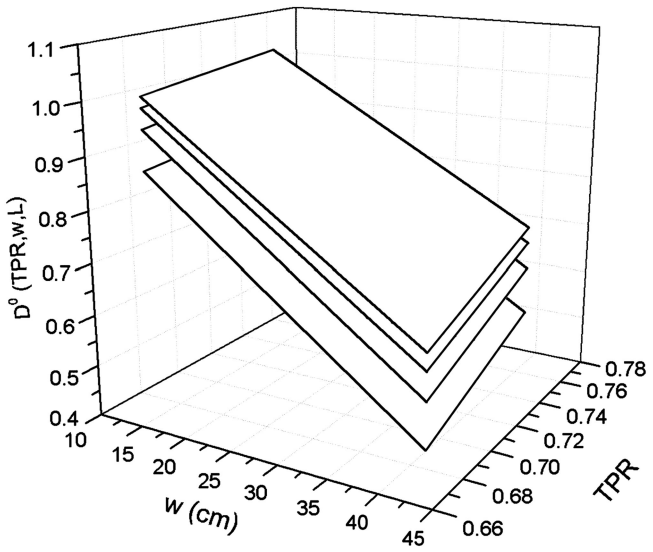

Figure 4: Surfaces obtained by fitting the doses $D^0(TPR,w,L)$ as a function of TPR for some square fields 4,10,16 and 20 cm^2.

An Example for the D_{iso} Determination

This example reports the application of equation [12] for the D_{iso} reconstruction in SWEP, using three values of TPR, w and L used in the experimental section. Moreover, the irradiation parameters are

- $w_{iso} = w/2$, this means d = 0 cm and both $f_{MV}(d,L) = 1$ and $TMR_{w/2}^{w_{iso}} = 1$
- 100 MU delivered with the clinical MU rate. This way $k_{lin} = 1$

uncertainty factors, ε, can be associated with to the k_0 and k_s factors due to the tolerance levels of the beam output factor reproducibility, $\varepsilon_0 = 2\%$ and the EPID signal reproducibility, $\varepsilon_s = 2\%$.

This way equation [12] can be rewritten with, $k_s\varepsilon_s$, and, $k_0\varepsilon_0$ for an integral signal, $S_t = 100 \times s_t(w,L)$

$$D_{iso} = 100 \times s_t(w,L) \frac{k_s \varepsilon_s}{k_0 \varepsilon_0} \left[\frac{D(w,L) \times k_0}{s_t(w,L) \times k_s} \right] \qquad [14]$$

Table III
k_s factors (equation 8) in terms of cCU/au obtained for the 9 beams of the three linacs examined in this work.

	Linac A	Linac B	Linac C
6 MV	$2.579 \cdot 10^{-5}$	$2.573 \cdot 10^{-5}$	$1.655 \cdot 10^{-5}$
10 MV	$2.840 \cdot 10^{-5}$	$2.832 \cdot 10^{-5}$	$2.025 \cdot 10^{-5}$
15 MV	$2.916 \cdot 10^{-5}$	$2.908 \cdot 10^{-5}$	$2.709 \cdot 10^{-5}$

Table IV
Average values k_{lin} for different MUs obtained for the three EPIDs used in this work.

	5 MU	20 MU	50 MU	100 MU	200 MU	400 MU
k_{lin}	1.016	1.011	1.008	1.000	0.997	0.994

that is equal to

$$D_{iso} = 100 \times D(w,L) \left(\frac{\varepsilon_s}{\varepsilon_0} \right) \qquad [15]$$

Of course, the isocenter dose is equal to the mid-plane dose D(w,L) (cGy/MU) for the specific beam, multiplied for the delivered 100 MU. The propagation of the two uncertainties can supply a global uncertainty of 3%.

Discussion and Conclusion

In this work some dosimetric characteristics of three aSi Elekta IviewGT EPIDs, as the signal reproducibility and the signal linearity with the MU, have been investigated. The short time signal, s, reproducibility was within ±1% (2 SD), while the long term signal reproducibility could be maintained well-within ±2% (2 SD). Moreover, the s signal showed a good linearity with the MU well-within ± 1% in the range between 20 MU and 400 MU (Table IV). However, it is suggested to verify the linearity of each EPID in order to evaluate if the k_{lin} correction factors can be neglected.

A calibration procedure for the aSi EPIDs of the Elekta linacs has been reported and for the three beams 6, 10 and 15 MV, a set of generalized signals s^0_t(TPR, w, L) have been determined. The generalized correlation ratios $F^0(TPR,w,L)$ by equations [10] and [11], as the set of $f_{MV}(d,L)$ factors avoid to perform the measurements in solid water-equivalent phantoms (that generally require about 10 hours for every linac) needed to implement the *in vivo* method.

A home-made software has been implemented to supply the isocenter dose D_{iso} for every beam of the patient once determined, (i) the patient's parameters L, w, w_{iso}, d and (ii) the linac correction factors, k_s, k_0 and k_{lin}.

The accuracy of the *in vivo* dosimetry method was well-discussed in a previous paper.(3) Propagating in quadrature the principal uncertainties (in terms of 2 SD), the total uncertainties equal to ±3.5% for head and pelvic tumours, and equal to ±5.0% for thorax tumors, were obtained. Moreover, reporting the results of the *in vivo* dosimetry in terms of the ratio $R = D_{iso}/D_{iso,TPS,}$ between the *in vivo* reconstructed isocenter dose, D_{iso}, and the TPS computed isocenter dose, $D_{iso,TPS}$, this latter determined with an uncertainty of ±3.5%

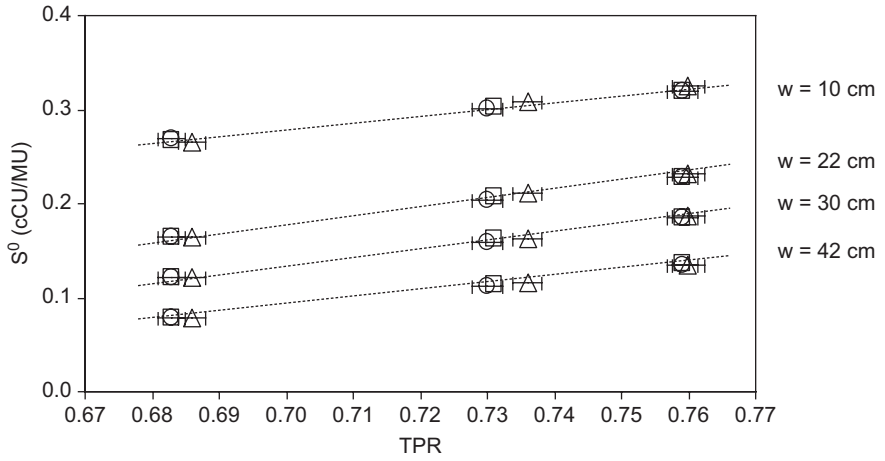

Figure 5: s^0_t(TPR,w,L) values and the linear fits obtained for w = 10,22,30 and 42 cm as a function of TPR for the 16 × 16 cm^2 square field.

(2 SD), global accuracy levels ranging between 5 % for head and pelvic and 6 % for thorax radiotherapy treatments were estimated. We suggest to choose the tolerance level coincident with the accuracy level according to the philosophy that any deviation larger than the accuracy level must be investigated to determine possible errors in (i) patient set-up, (ii) machine settings, (iii) TPS calculations and (iv) the patient's morphology changes. These tolerance/action levels seem to be more restrictive than the ones reported by ESTRO (1) for the practical method that uses diodes, where for the same treatments, the tolerance/action levels, only for the entrance doses, have been fixed in that report in 5% and 8% for pelvic and thorax radiotherapy, respectively. As respect to other works (16, 17) that report the same accuracy level for the dose at a reference depth (5 cm), the method here reported supplies the dose in the tumor at the isocenter point that is generally used as the reference point (18).

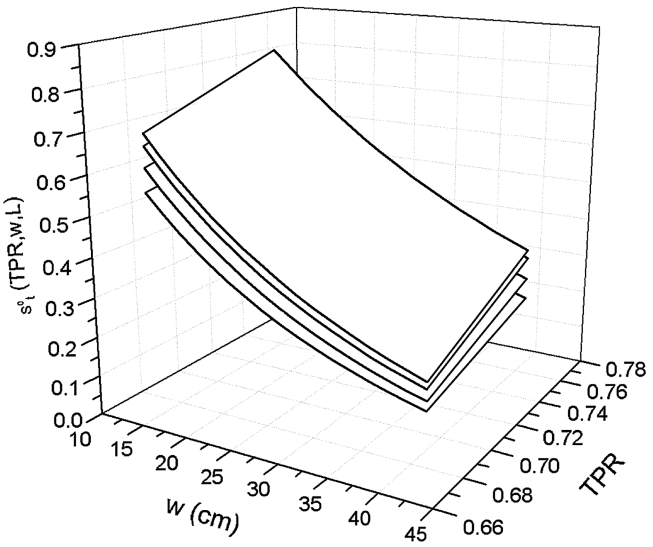

Figure 6: Surfaces obtained by fitting the transit signals s^0_t(TPR,w,L) as a function of TPRs for the some square fields 4,10,16 and 20 cm^2.

Even if the proposed method is not an independent check of the dosimetry because it requires some of the parameters used by the TPS, it was demonstrated, (3) that the method is able to check, (i) incorrect patient positioning (ii) inconsistent CT calibration number, (iii) the patient's morphological modifications. About the morphological tissue changes for lung tumors during the treatment, the method has been used for a dosimetry-guided radiotherapy that can be well-integrated with the image-guided radiotherapy (19). Indeed, the change of the transit signals due to the morphological changes of the tumor and the lung tissues that present large different densities can be well-detected. Using this aspect, the method was recently also used for a real time control of the $D_{iso,TPS}$ during the breath-hold technique adopted to reduce the lung tumor motion (20).

In conclusion, the method seems to be accurate and practical because it avoids specific measurements in solid water-equivalent phantoms in the centers. At the moment, the authors are studying the possibility to obtain the reconstruction in real time after the treatment and to extend this generalized procedure also to aSi EPIDs and linacs by other manufacturers.

Conflict of Interest

We certify that regarding this paper, no actual or potential conflicts of interests exist; the work is original, has not been accepted for publication nor is concurrently under consideration elsewhere, and will not be published elsewhere without the permission of the Editor and that all the authors have contributed directly to the planning, execution or analysis of the work reported or to the writing of the paper.

References

1. ESTRO Practical guidelines for the implementation of in vivo dosimetry radiotherapy with photon beams (entrance dose). Physics for clinical radiotherapy. Booklet n.5 2001.

2. van Elmpt, W., McDermott, L., Nijsten, S., Wendling, M., Lambin, P., Mijnheer, B. A literature review of electronic portal imaging for radiotherapy dosimetry. *Radiother Oncol* 88, 289-309 (2008).
3. Parker, B. C., Shiu, A., White, R. A., Maor, M., Dong, L., Liu, H. H. Pre-treatment verification of IMSRT using electronic portal imaging and Monte Carlo calculation. *Technol Cancer Res Treat 8*, 413-424 (2009).
4. Van Esch, A., Depuydt, T., Huyskens, D. P. The use of an aSi-based EPID for routine absolute dosimetric pre-treatment verification of dynamic IMRT fields. *Radiother Oncol 71*, 223-34 (2004).
5. Piermattei, A., Fidanzio, A., Azario, L., Grimaldi, L., D'Onofrio, G., Cilla, S., Stimato, G., Gaudino, D., Ramella, S., D'Angelillo, R., Cellini, F., Trodella, L., Russo, A., Iadanza, L., Zucca, S., Fusco, V., Di Napoli, N., Gambacorta, M. A., Balducci, M., Cellini, N., Deodato, F., Macchia, G., Morganti, A. G. Application of a practical method for the isocenter point in-vivo dosimetry by a transit signal. *Phys Med Biol 52*, 5101-17 (2007).
6. McDermott, L. N., Louwe, R. J. W., Sonke, J. J., van Herk, M., Mijnheer, B. J. Dose-response and ghosting effects of an amorphous silicon electronic portal imaging device. *Med Phys 31*, 285-95 (2004).
7. Winkler, P., Hefner, A., Georg. D. Dose-response characteristics of an amorphous silicon EPID. *Med Phys 32*, 3095-3105 (2005).
8. IAEA (International Atomic Energy Agency) Absorbed dose in external beam radiotherapy: an international code of practice for dosimetry based on standards of absorbed dose to water IAEA TRS 398 (2004).
9. Piermattei, A., Grimaldi, L., D'Onofrio, G., Cilla, S., Viola, P., Craus, M., Fidanzio, A., Azario, L., Deodato, F., Macchia, G., Morganti, A. G. In-vivo portal dosimetry by an ionization chamber. *Physica Medica* XXI (4), 143-52 (2005).
10. Piermattei, A., Fidanzio, A., Stimato, G., Azario, L., Grimaldi, L., D'Onofrio, G., Cilla, S., Balducci, M., Gambacorta, M. A., Di Napoli, N., Cellini, N. In vivo dosimetry by an aSi-based EPID. *Med Phys 33*, 4414-22 (2006).
11. IviewGT 2006 User Manual Elekta Limited.
12. TableCurve 3D Ver. 4.Systat Software, Inc., CA, USA (2004).
13. Schneider, U., Pedroni, E., Lomax, A. The calibration of CT Hounsfield units for radiotherapy treatment planning. Phys. *Med Biol 41*, 111-24 (1996).
14. Sterling, T. D., Perry, H., Katz, L. Automation of radiation treatment planning IV. *Brit J Radiol 37*, 544-50 (1964).
15. Louwe, R. J., McDermott, L. N., Sonke, J. J., Tielenburg, R., Wendling, M., van Herk, M. B., Mijnheer, B. J. The long-term stability of amorphous silicon flat panel imaging devices for dosimetry purposes. *Med Phys 31*, 2989- 2995 (2004).
16. Pasma, K. L., Kroonwijk, M., Quint, S., Visser, A. G., Heijmen, B. J. Transit dosimetry with an electronic portal imaging device (EPID) for 115 prostate cancer patient. *Int J Radiat Oncol Biol Phys 45*, 1297-3003 (1999).
17. Nijsten, S. M., Mijnheer, B. J., Dekker, A. L., Lambin, P., Minken, A. W. Routine individualised patient dosimetry using electronic portal imaging devices. *Radiother Oncol 83*, 65-75 (2007).
18. Report 62. Prescribing, Re-cording and Reporting Photon Beam Therapy. (Supplement to ICRU Report 50)" (1999).
19. Piermattei, A., Cilla, S., Grimaldi, L., Sabatino, D., Fidanzio, A., Greco, F., Mameli, A., Balducci, M., Mattiucci, G. C., Frascino, V., Stimato, G., Gaudino, D., Ramella, S., Trodella, L., D'Onofrio, G., Zini, G., Macchia, G., Digesù, C., Morganti, A., G., Clemente, S., Cozzolino, M., Pedicini, P., Fusco, V. Integration between in-vivo dosimetry and image guided radiotherapy for lung tumors. *Medical Physics 36*, 2206-14 (2009).
20. Piermattei, A., Cilla, S., Grimaldi, L., Viola, P., Frattarolo, L., D'Onofrio, G., Craus, M., Fidanzio, A., Azario, L., Greco, F., Digesù, C., Deodato, F., Macchia, G., Morganti, A. G. Real time dosimetry reconstruction for the breath hold radiotherapy technique: an initial experience. *Acta Oncologica 47*, 1414-1421 (2008).

Appendix A: Coefficients for equations 13, 10 and 11 in the text.

Table A1

Coefficients f_1 of the fits performed for the $f_{MV}(d,L)$ factors as a function of the distance, d, (equation 13) and for the three megavoltage beams.

	Square field side (cm)					
	4	8	10	12	16	20
6 MV	-7.989E-04	-1.897E-03	-2.642E-03	-3.386E-03	-4.598E-03	-5.933E-03
10 MV	-1.654E-03	-2.553E-03	-3.208E-03	-3.864E-03	-4.316E-03	-5.775E-03
15 MV	-1.673E-03	-3.175E-03	-3.886E-03	-4.598E-03	-5.456E-03	-6.250E-03

Table A2

Coefficients a_i (I = 1,…,6) of the polynomial surface fits for D^0 (equation 10) for the six square field sides (L × L cm^2).

Coefficient index	4 × 4	8 × 8	10 × 10	12 × 12	16 × 16	20 × 20
a_1	1.35829E+00	1.66047E+00	1.77903E+00	1.56038E+00	1.26118E+00	1.88206E+00
a_2	-3.89879E-02	-3.67915E-02	-3.51922E-02	-3.55092E-02	-3.38512E-02	-3.27646E-02
a_3	-1.22685E+00	-2.01130E+00	-2.29958E+00	-1.59924E+00	-6.80369E-01	-2.26615E+00
a_4	9.90741E-05	5.64815E-05	4.02778E-05	3.14815E-05	1.55093E-05	3.00926E-06
a_5	1.06570E+00	1.65613E+00	1.84033E+00	1.31302E+00	6.37265E-01	1.65519E+00
a_6	3.01252E-02	3.02655E-02	2.95331E-02	3.08375E-02	3.02214E-02	3.01669E-02

Table A3
Coefficients b_i (I = 1,…,10) of the polynomial surface fits for s^0_t (equation 11) for the six square field sides (L × L cm^2).

Coefficient index	4 × 4	8 × 8	10 × 10	12 × 12	16 × 16	20 × 20
b_1	1.81339E+02	1.46791E+02	1.80070E+02	1.20870E+02	2.26741E+02	2.03795E+02
b_2	1.06355E-01	9.49833E-02	5.08104E-02	3.68842E-02	6.71633E-02	2.70425E-02
b_3	-7.59169E+02	-6.14951E+02	-7.49692E+02	-5.04410E+02	-9.45312E+02	-8.47320E+02
b_4	1.64812E-03	1.37235E-03	1.72799E-03	1.34544E-03	1.25453E-03	1.56237E-03
b_5	1.06277E+03	8.62054E+02	1.04396E+03	7.04919E+02	1.31632E+03	1.17763E+03
b_6	-4.68058E-01	-4.21030E-01	-3.24999E-01	-2.56086E-01	-3.34568E-01	-2.49264E-01
b_7	-5.63220E-06	-4.14140E-06	-5.83620E-06	-4.38080E-06	-4.31860E-06	-4.32440E-06
b_8	-4.95105E+02	-4.01812E+02	-4.83628E+02	-3.27226E+02	-6.09431E+02	-5.44300E+02
b_9	3.73598E-01	3.31875E-01	2.77814E-01	2.12960E-01	2.62765E-01	2.22932E-01
b_{10}	-1.30443E-03	-1.05993E-03	-1.37283E-03	-9.94610E-04	-8.75270E-04	-1.32555E-03

Received: February 10, 2010; Revised: June 30, 2010;
Accepted: July 30, 2010